

Evidence for coupling between exciton emissions and surface plasmon in Ni-coated ZnO nanowires

Qijun Ren, Stanislav Filippov, Shula Chen, M. Devika, N. Koteeswara Reddy, C. W. Tu, Weimin Chen and Irina Buyanova

Linköping University Post Print

N.B.: When citing this work, cite the original article.

Original Publication:

Qijun Ren, Stanislav Filippov, Shula Chen, M. Devika, N. Koteeswara Reddy, C. W. Tu, Weimin Chen and Irina Buyanova, Evidence for coupling between exciton emissions and surface plasmon in Ni-coated ZnO nanowires, 2012, Nanotechnology, (23), 42, 425201.

<http://dx.doi.org/10.1088/0957-4484/23/42/425201>

Copyright: Institute of Physics

<http://www.iop.org/>

Postprint available at: Linköping University Electronic Press

<http://urn.kb.se/resolve?urn=urn:nbn:se:liu:diva-85481>

Evidence for coupling between exciton emissions and surface plasmon in Ni coated ZnO nanowires

Q J Ren¹, S Filippov¹, S L Chen¹, M Devika², N Koteswara Reddy^{2,i}, C W Tu^{2,3}, W M Chen¹ and I A Buyanova^{1*}

¹ Department of Physics, Chemistry and Biology, Linköping University 58183, Linköping, Sweden

² Department of Nanobio Materials and Electronics, Gwangju Institute of Science and Technology, Gwangju 500712, Republic of Korea

³ Department of Electrical and Computer Engineering, University of California, La Jolla, California 92093-0407, USA

*E-mail: irb@ifm.liu.se

Abstract

We show that coating ZnO nanowires (NWs) with a transition metal, such as Ni, can increase efficiency of light emission at room temperature. Based on detailed structural and optical studies, this enhancement is attributed to energy transfer between near-band-edge emission in ZnO and surface plasmons in the Ni film which leads to an increased rate of the spontaneous emission. It is also shown that the Ni coating leads to an enhanced non-radiative recombination via surface states, which becomes increasingly important at low measurement temperatures and in annealed ZnO/Ni NWs.

PACS numbers: 73.21.-b, 78.68.+m, 77.55.hf, 78.67.Uh

1. Introduction

ⁱ Present address: Center for Nanoscience and Engineering, Indian Institute of Science, Bangalore-12, India

ZnO nanowires (NWs) have in recent years attracted considerable research interest as a promising material system for novel functional devices. Due to large lateral surfaces, which facilitate efficient strain relaxation, ZnO NWs and other nanostructures can be grown with a low defect density [1] on a vast variety of substrates. The high material quality combined with a wide and direct band gap, large exciton binding energy, and ability to control their nucleation sites, makes NWs attractive for applications in optoelectronic devices such as ultraviolet lasers [2], light emitting diodes [3] as well as for white lighting. Moreover, when alloyed with transition metals (TMs) such as Ni, Cr, Mn, etc, ZnO is predicted and demonstrated to exhibit ferromagnetic properties at and above room temperature [4, 5]. This makes it a promising candidate for future devices with spin-enable functionality, e.g. spin-polarized light sources. However, doping with TM often degrades intensity of near-band-edge (NBE) emissions in ZnO [6, 7], and hence hinders this material from photonic applications.

A possible approach to circumvent this degradation is coating ZnO NWs with TM particles with the purpose to enhance their radiative efficiency by utilizing the interaction of excitons in ZnO and surface plasmons (SP) arising from collective electron excitation in TM. Such SP-mediated emission has recently been demonstrated in ZnO nanostructures coated by various metals (Ag, Au, Ti, Al and Pt) and dramatic enhancement of the NBE emission was observed [8-12]. It should also be possible to realize the SP-exciton coupling in TM capped ZnO NWs as TMs support SP modes at their surfaces. Despite that the proof of this concept may lead to promising applications of ZnO/TM systems in spin based optical devices, no work on this issue has so far been reported in the literature. The purpose of this work is to understand effects of TM coating and to explore the SP-exciton coupling in ZnO/Ni core/shell NWs, by means of optical spectroscopy supported by structural analysis. Ni was chosen here as TM because its fundamental SP mode closely matches in energy with the NBE emission in ZnO.

2. Experimental

The studied ZnO NWs were grown on Au coated sapphire substrates using rapid thermal chemical vapor deposition (RTCVD) at 950 °C. The growth was performed at pressure of 20 Torr

under the Ar and O₂ flow. ZnO NWs were then capped by a 10 nm-thick Ni film deposited at room temperature (RT) using e-beam evaporation. After the coating, some of the ZnO/Ni core/shell NWs were annealed in the RTCVD chamber at 400 °C for 5 minutes. Structural and chemical properties of the samples were evaluated by scanning electron microscopy (SEM), X-ray diffraction (XRD), transmission electron microscopy (TEM), and selected area electron diffraction (SAED). Time resolved PL measurements (TR PL) were performed at 4 and 300 K. PL was excited by third-harmonic pulses of a mode-locked Ti:sapphire laser, with an excitation wavelength of 285 nm and a repetition rate of 80 MHz. The PL from the samples was then recorded by a streak camera system with an overall time resolution of about 20 ps. To account for reflection and absorption of the excitation light in the 10 nm-thick Ni shell layer, intensities of the PL emission measured from the ZnO/Ni structures were calibrated to the same effective excitation power as that used for the bare ZnO NWs. A calibration factor of 4 was applied, which is deduced based on tabulated reflection and absorption coefficients of Ni [13]. Resonant Raman scattering measurements were done using a micro-Raman system with a He-Cd excitation laser (325 nm). The spectra were acquired at RT in the back-scattering geometry.

3. Structural properties of ZnO/Ni core-shell nanowires

Representative SEM images from the bare ZnO NWs and coated ZnO/Ni NWs are shown in figure 1(a) and (b), respectively. It is found that the NWs are rather uniform in size and have an average diameter of around 100 nm. They are preferentially vertically aligned and have smooth surface morphology, which indicates their good crystalline quality.

The good structural quality was also confirmed by XRD measurements, as shown in figure 2. The XRD spectra from the as-grown ZnO NWs (figure 2(a)) are found to have a full width at half maximum (FWHM) of 0.27°, indicative of high quality ZnO. The NWs are preferentially oriented along the <001> direction, since the calculated d-spacing of the major peak ($2\theta = 34.4^\circ$, $d = 0.261$ nm) matches the hexagonal ZnO. The XRD peaks at 31.98° and 41.4° are due to Au catalyst and sapphire substrate, respectively. Judging from the FWHM of the main ZnO peak (denoted as “ZnO (002)” in figure 2), crystalline quality of ZnO remains superior after Ni coating and also after post-annealing. In

addition, Ni coating causes an appearance of an additional diffraction peak at 41.7° (see figure 2(b) and 2(c)), which belongs to hexagonal (002) Ni phase [14]. For the ZnO/Ni NWs annealed at 400°C , two new peaks at 56.62° and 56.79° appear in the spectra and originate from hexagonal ZnO (110) and hexagonal Ni_2O_3 (202) phase, respectively [14]. This implies a small amount of oxidation of Ni under high temperature annealing.

To further evaluate the crystalline properties of the three structures, high resolution TEM (HRTEM) as well as SAED measurements were performed and representative results are shown in figure 3. They again confirm that the ZnO NWs are grown along the $\langle 001 \rangle$ direction since the calculated d-spacing values from the Fast Fourier Transform (FFT) of HRTEM is found to be 0.261 nm. The SAED studies (figure 3(b)) confirm these results and show that the bare ZnO NWs are clearly single-crystalline. Figure 3(c) and 3(d) depict the HRTEM and SAED images of the as-grown ZnO/Ni NWs. From HRTEM studies we can see that the thickness of the as-deposited Ni nanolayer over ZnO NWs is about 10 nm and is rather uniform (inset in figure 3(c)). The FFT analysis of the HRTEM image shows that the as-deposited Ni nanolayer contains two distinguishable hexagonal nanocrystals oriented along the [001] and [010] directions, respectively (see figure 4). The SAED analysis of the as-grown ZnO/Ni core-shell structures (figure 3(d)) clearly confirms the HRTEM results and is also consistent with the XRD data. Thus, the as-deposited Ni layers on the hexagonal facets of the ZnO NWs are composed of fine hexagonal polycrystalline nanocrystals oriented along the [001] and [010] directions. However, after annealing at 400°C , the polycrystalline Ni nanocrystals start to merge together and form a more uniform Ni nano-film, as is shown in figure 3(e). From the SAED image (figure 3(f)) we can also observe that the polycrystalline Ni phase converts to the single-crystalline phase after annealing.

4. Effects of Ni coating on optical properties of ZnO nanowires

Let us now evaluate optical properties of the ZnO/Ni core/shell NWs. Figure 5(a) shows effects of Ni coating and thermal annealing on RT PL spectra from the investigated structures. The PL spectrum of the ZnO NWs exhibits intense NBE emission due to radiative recombination of free

excitons (FXs) with only a marginal contribution of defect-related emissions within the visible spectral range, indicative of superior optical quality. The intensity of the FXs emission is found to be further enhanced after Ni coating but is, however, suppressed after subsequent annealing at 400°C. At 4K, the PL spectra from all structures contain several excitonic emissions due to recombination of donor bound excitons (BXs) and surface excitons (SX) – see figure 5(b). The same emissions are also detected in the Ni-coated structures without appearance of additional features, which implies that the coating does not lead to unintentional doping of impurities such as H in ZnO. At 4K, however, a decrease of the PL intensity after Ni coating is observed even in the as-grown structure. The results presented in figure 5 imply that several counteracting mechanisms affect efficiency of the radiative recombination in the ZnO/Ni NWs upon capping and annealing.

Let us first discuss the origin of the PL enhancement observed at RT in the as-grown ZnO/Ni NWs. The first possible reason for this effect could be surface passivation. It has been reported [15] that capping of ZnO surfaces with dielectric or metal films may cause a reduction of density of surface recombination centers that lead to an increase of the NBE emission. Alternatively, it may be related to coupling between the spontaneous emission of the NBE excitons in ZnO and SPs of the Ni metal. This SP-exciton interaction at the metal/ZnO interface may occur when the SP energy is comparable with the ZnO band gap energy. To evaluate feasibility of the SP formation at the Ni/ZnO interface, we have calculated the SP dispersions for Ni/ZnO and Ni/air interfaces using the known relation [16, 17]

$$\hbar k_{SP} = \frac{\hbar \omega}{c} \sqrt{\frac{\epsilon_{Ni} \epsilon_d}{\epsilon_{Ni} + \epsilon_d}} \quad (1)$$

Here k_{SP} is the SP wave vector, $\hbar \omega$ the incident energy, c the speed of light, and ϵ_{Ni} and ϵ_d are the dielectric functions of Ni and dielectric medium (i.e. air or ZnO), respectively [13, 18]. The calculated dispersions are shown in the inset in figure 5(a). Since the energies of the NBE emission in ZnO lie between the SP energies for the Ni/ZnO and Ni/air interfaces, the resonant coupling of emitting light with surface plasmon is highly probable for suitable sizes of Ni nanoparticles [19]. The SPs could couple to photons again by scattering and light is then extracted into free space due to the roughness and imperfections of the Ni surfaces, leading to an enhancement of the detected light emission.

In order to determine which mechanism dominates in the investigated structures, we have analyzed transient properties of the monitored emissions. Representative PL decays measured at RT from the bare ZnO and Ni-coated ZnO/Ni NWs are summarized in figure 6(a). In the bare ZnO NWs, the PL decay is found to be biexponential and contain fast and slow components with their respective time constants of $\tau_f=0.45$ ns and $\tau_s=3$ ns. The fast component is commonly attributed [20, 21] to lifetime of excitons located in the direct proximity to the surface and can, therefore, be shortened due to recombination via surface states. The slow component, on the other hand, likely represents the “true” exciton lifetime. The most prominent effect of the Ni coating in the PL transient is significant shortening of the exciton lifetimes with $\tau_f(\tau_s)=0.1$ (0.43) ns detected from the as-grown ZnO/Ni NWs. This clearly shows that surface passivation due to Ni coating is not responsible for the enhanced PL efficiency. Indeed, suppression of efficient non-radiative recombination via the surface states should lead to longer decay times of the NBE emission which is contrary to the experimental data shown in figure 6(a). We, therefore, attribute the observed PL enhancement to the SP-exciton coupling in the Ni capped ZnO/Ni NWs. Within this scenario, excitons recombine and transfer energy into the SP modes instead of free space. The interaction between the SPs and the excitons greatly enhances rates of the spontaneous emission in the ZnO NWs, which leads to the observed increase of the emission intensity accompanied by the shortening of the exciton lifetime (or emission decay time).

We should note that an alternative explanation to the enhanced emission as a result of enhanced absorption of the excitation light due to the field enhancement can be ruled out here. This is because in our case the excitation light field is hard to couple to the SP modes of Ni due to the energy mismatch. The calculated SP dispersion of the Ni film shows that the SP energy is below 4 eV (see the inset of figure 5(a)), which is well below the excitation photon energy of 4.35 eV. Although the non-resonant coupling is also possible, the coupling strength should be much weaker and negligible. Moreover, if the local excitation field (and thus the absorption of ZnO) is enhanced, it should not have any effect on the exciton lifetime since it does not change the exciton radiative transition rates according to Fermi’s Golden rule.

In principle, the SP-mediated PL enhancement is in analogy to the Purcell effect in cavity

quantum electrodynamics where excitons are coupled to cavity photons [22]. The Purcell factor, F_P , quantifies the coupling-induced increase in the rate of spontaneous emission. Therefore, it can be calculated [23] based on the measured PL decay times in the bare and Ni-coated ZnO NWs as $F_P = \tau_s^{ZnO} / \tau_s^{Ni/ZnO} \sim 7$, under the assumption that the shortening of the exciton lifetime in the coated structure is solely induced by the SP-exciton coupling. This expected PL enhancement is substantially larger than that observed experimentally. This may indicate that either Ni coating also induces surface states, which act as competing non-radiative (NR) recombination centers degrading optical efficiency, or SPs within the continuous Ni film partly dissipate non-radiatively. The latter effect is shown to be important in Au-coated ZnO nanorods [9] when the deposited metallic nanoparticles merged into a continuous film.

From figure 5(b), the SP-mediated enhancement of the PL emission in the as-grown ZnO/Ni NWs is no longer observed at 4K. The same effect has also been reported for InGaN/GaN quantum wells [19, 24]. A possible reason for this decrease is a weaker coupling between the SPs and the BX emissions that dominate the PL spectra at 4K. Indeed, in the dipole approximation the recombination rate of the excitons into the plasmon continuum depends both on the dipole moment (or collective oscillator strength) of the excitons and on the SP density of states at the exciton energy. The oscillator strength of the BX transitions is significantly lower than that of the FX [25], which should lead to their weaker coupling with the SPs. Moreover, localization of the BX may further decrease probability of their scattering into the SPs as compared with the FXs that are highly mobile [26]. As a result, the detrimental effect of the enhanced surface recombination becomes predominant leading to the observed decrease in the PL intensity in the Ni-coated structures. We note that the Ni-induced surface recombination seems to mainly occur via non-radiative processes to account for the observed quenching of the SX emission. The suggested scenario is also consistent with the results of the TR PL measurements – figure 6(b). The PL decays measured at 4K from both bare ZnO and as-grown ZnO/Ni structures are dominated by the fast decay component with $\tau_f = 0.23$ ns and 0.2 ns, respectively, whereas τ_s is about 1 ns for both structures. This means that the Purcell factor decreases to 1 at 4K or, in other words, that the SP-exciton coupling is strongly suppressed. The contribution of the fast decay component to the total PL decay is more pronounced in the Ni-coated structure, confirming the higher

rate of the NR recombination.

From figures 5 and 6, the competing NR recombination process becomes more severe after post-growth annealing. This is evident from both the low intensity of the NBE emission and very short PL decay times detected at RT and 4K in the annealed ZnO/Ni NWs. Several effects likely contribute to the observed degradation. First of all, annealing can facilitate diffusion of Ni atoms into sub-surface regions of the ZnO NWs thus extending the spatial regions with severe NR recombination. Moreover, since annealing also changes the crystalline structure of the Ni coating from Ni nanoparticles to single-crystalline Ni film, which has been clearly revealed from our HRTEM and SAED study, the localized SP modes from Ni nanoparticles may be replaced by the propagating SP modes. This would cause a reduction of the coupling of the spontaneous emission with the SPs, as well as a reduction of the external light extraction efficiency due to momentum mismatch between the photons and the SPs.

Evidence for efficient coupling with UV light within the range of the SP dispersion of the Ni film in the ZnO/Ni core/shell NWs was also obtained from resonant Raman scattering measurements. Figure 7 shows Raman scattering spectra measured from the investigated ZnO NWs before and after Ni coating. For all samples, the spectra contain a number of peaks spaced by about 572 cm^{-1} due to the first- and multiple-order Raman scattering involving longitudinal optical (LO) phonons, as well documented in the literature [26]. Remarkably, the Raman intensity is significantly enhanced in the Ni-coated ZnO NWs, e.g. by about one order of magnitude in the as-grown ZnO/Ni NW,, which provides an independent proof for the coupling of light with the SPs in the Ni film. The observed enhancement is somewhat weaker in the annealed structure, consistent with the results from the PL measurements discussed above.

5. Conclusions

In conclusion, we have investigated effects of Ni coating and subsequent annealing on optical properties of ZnO NWs by using time-resolved PL spectroscopy and Raman spectroscopy complemented by structural analytic techniques. The PL efficiency is found to be strongly influenced by two counteracting effects, i.e. (i) coupling of the emitted light with the SPs in the Ni film that enhances the light emission and (ii) enhanced NR recombination via surface states induced by the Ni

coating that suppresses the light emission. The former effect is found to dominate at RT in the as-grown ZnO/Ni core/shell structures but is strongly suppressed at low temperatures and also in the annealed ZnO/Ni NWs. The coupling of the UV light within the spectral dispersion of the SPs is also independently confirmed by the observed strong increase of the Raman scattering signals in the Ni-coated structures. Our results provide a direct proof that SP-mediated enhancement of light emission can be achieved in the ZnO/TM systems which is promising for future efficient optical emitters with spin-enabling functionality.

Acknowledgements

Financial support by the Swedish Research Council (grant # 621-2010-3971) and by the World-Class University Program through NRF grant funded by the Korea government (MEST) (grant # R31-10026) is greatly appreciated. We are also grateful J.-W. Kang at GIST for lab assistance.

References

- [1] Robin I C, Gauron B, Ferret P, Tavares C, Feuillet G, Dang L S, Gayral B and Gerard J M 1995 *Appl. Phys. Lett.* **91** 143120
- [2] Huang M H, Mao S, Feick H, Yan H Q, Wu Y Y, Kind H, Weber E, Russo R and Yang P D 2001 *Science* **292** 1897
- [3] Lim J H Kang C K, Kim K K, Park I K, Hwang D K and Park S J 2006 *Adv. Mater.* **18** 2720-24
- [4] Yi J B *et al* 2010 *Phys. Rev. Lett.* **104** 137201
- [5] Dietl T, Ohno H, Matsukura F, Cibert J and Ferrand D 2000 *Science* **287** 1019
- [6] Jin Z *et al* 2001 *Appl. Phys. Lett.* **78** 3824
- [7] Wang Y S, Thomas P J and O'Brien P 2006 *J. Phys. Chem B* **110** 21412-15
- [8] Lawrie B J, Haglund R F Jr and Mu R 2009 *Opt. Express* **17** 2565-72
- [9] Cheng C W, Sie E J, Liu B, Huan C H A, Sum T C, Sun H D and Fan H J 2010 *Appl. Phys. Lett.* **96** 071107
- [10] Liu K W, Tang Y D, Cong C X, Sum T C, Huan A C H, Shen Z X, Wang L, Jiang F Y, Sun X W and Sun H D 2009 *Appl. Phys. Lett.* **94** 151102
- [11] Song J, An X, Zhou J, Liu Y, Wang W, Li X, Lan W and Xie E 2010 *Appl. Phys. Lett.* **97** 122103
- [12] Ni W H, An J, Lai C W, Ong H C and Xu J B 2006 *J. Appl. Phys.* **100** 026103
- [13] Light absorption within the Ni film was calculated based on the known absorption and reflection coefficients of Ni taken from Lynch D W and Hunter W R 1985 *Handbook of Optical Constants of Solids*, ed E D Palik (London: Academic)
- [14] JCPDS data of ZnO #36-1451; JCPDS data of Ni #45-1027; JCPDS data of Ni₂O₃ #14-0481.
- [15] Richters J P, Voss T, Kim D S, Scholz R and Zacharias M 2008 *Nanotechnology* **19**

305202

[16] Lai C W, An J and Ong H C 2005 *Appl. Phys. Lett.* **86** 251105

[17] Barnes W L, Dereux A and Ebbesen T W 2003 *Nature* **424** 824

[18] Washington P L, Ong H C, Dai J Y and Chang R P H 1998 *Appl. Phys. Lett.* **72** 3261

[19] Okamoto K, Niki I, Shvartser A, Narukawa Y, Mukai T and Scherer A 2004 *Nature Mater.* **3** 601-5

[20] Lee S K, Chen S L, Dong H, Sun L, Chen Z, Chen W M and Buyanova I A 2010 *Appl. Phys. Lett.* **96** 083104

[21] Monemar B, Paskov P P, Bergman J P, Pozina G, Toropov A A, Shubina T V, Malinauskas T and Usui A 2010 *Phys. Rev. B* **82** 235202

[22] Purcell E M 1946 *Phys. Rev.* **69** 681

[23] Gérard J M, Sermage B, Gayral B, Legrand B, Costard E and Mieg V T 1998 *Phys. Rev. Lett.* **81** 1110

[24] Lu Y C, Chen C Y, Yeh D M, Huang C F, Tang T Y, Huang J J and Yang C C 2007 *Appl. Phys. Lett.* **90** 193103

[25] Chen S L, Chen W M and Buyanova I A 2011 *Phys. Rev. B* **83** 245212

[26] Liu Y P, Guo Y, Li J Q, Trunk M, Kuznetsov A Y, Xu J B, Mei Z X and Du X L 2011 *J. Opt.* **13** 075003

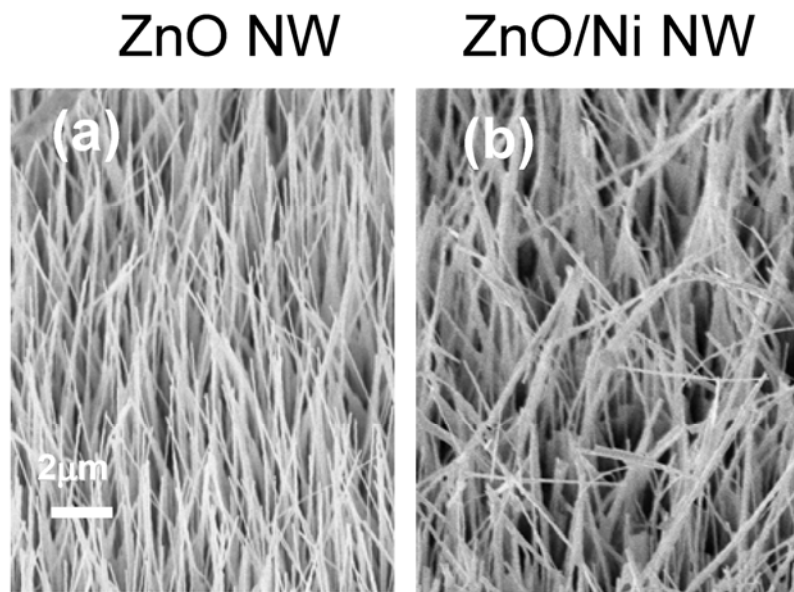


Figure 1. (a)-(b) Representative SEM images from the bare ZnO NWs and the as-grown ZnO/Ni core-shell NWs.

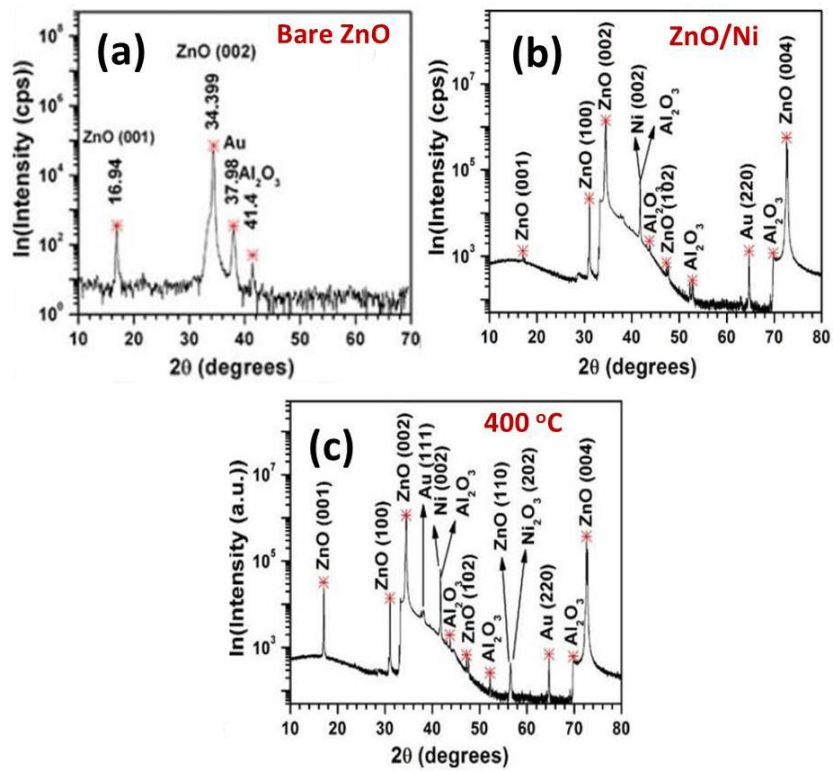


Figure 2. XRD spectra of (a) the bare ZnO NWs, (b) the as-grown ZnO/Ni NWs and (c) the ZnO/Ni NWs after annealing at 400 °C.

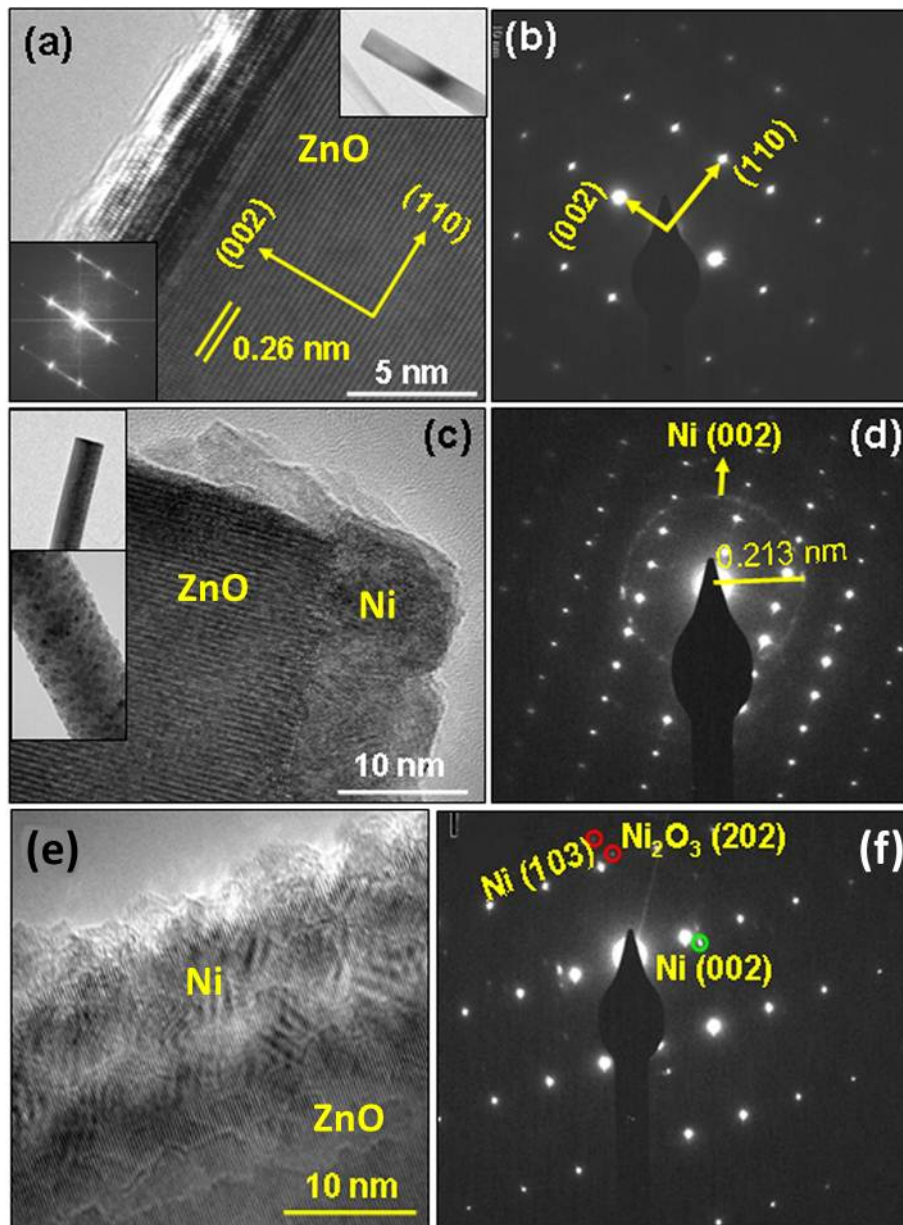


Figure 3. (a) HRTEM and (b) SAED images of the bare ZnO NWs. The upper and lower insets in (a) show a TEM image of a ZnO NW and FFT image taken from HRTEM. (c) and (e) are the HRTEM images of the as-grown and annealed ZnO/Ni NWs, respectively, whereas the corresponding SAED images are shown in (d) and (f). The insets in (c) show the TEM images of the as-grown Ni coated ZnO NWs.

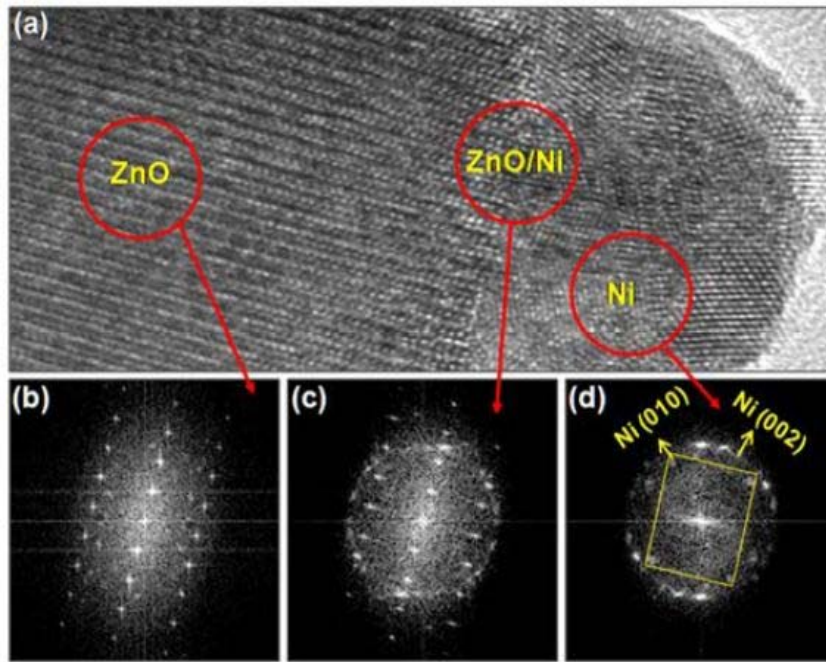


Figure 4. (a) HRTEM image of the as-grown ZnO/Ni NWs and (b-d) FFT images taken from different regions as indicated in (a).

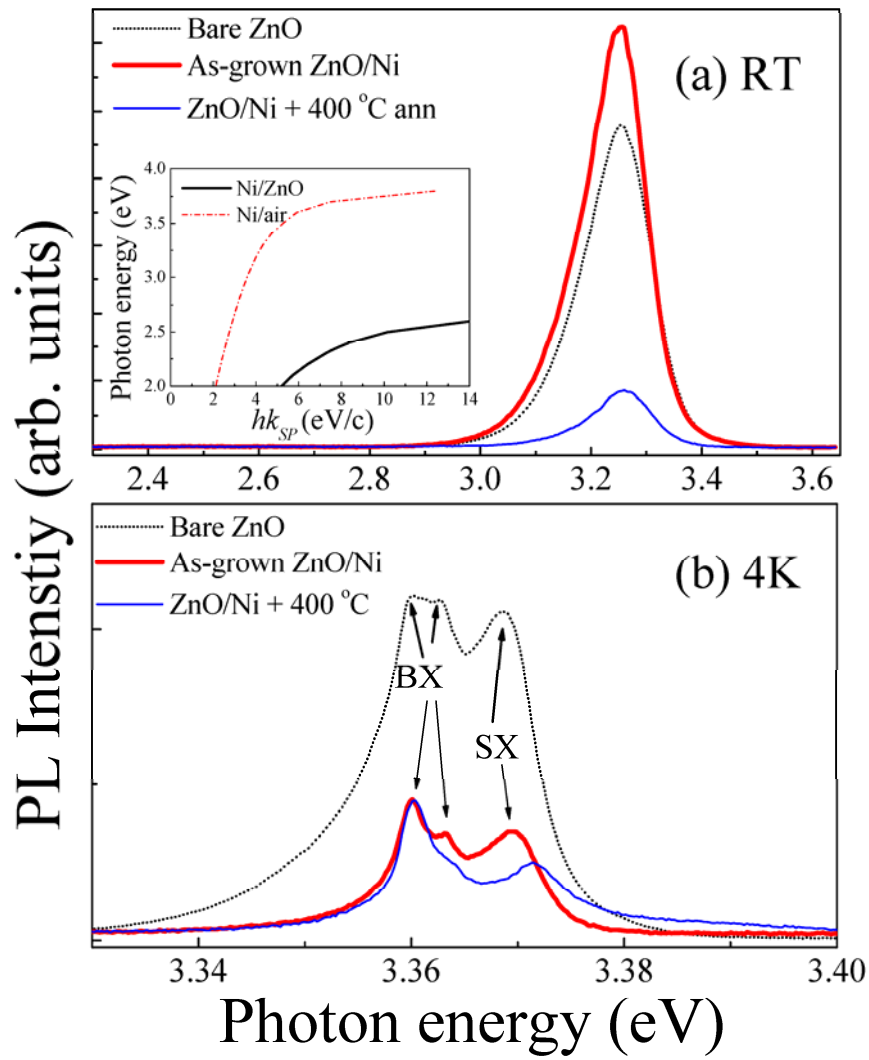


Figure 5. Representative PL spectra measured at room temperature (a) and 4K (b) from the ZnO NWs before and after Ni coating. The inset in (a) shows the calculated surface plasmon dispersions for Ni/ZnO and Ni/air interfaces.

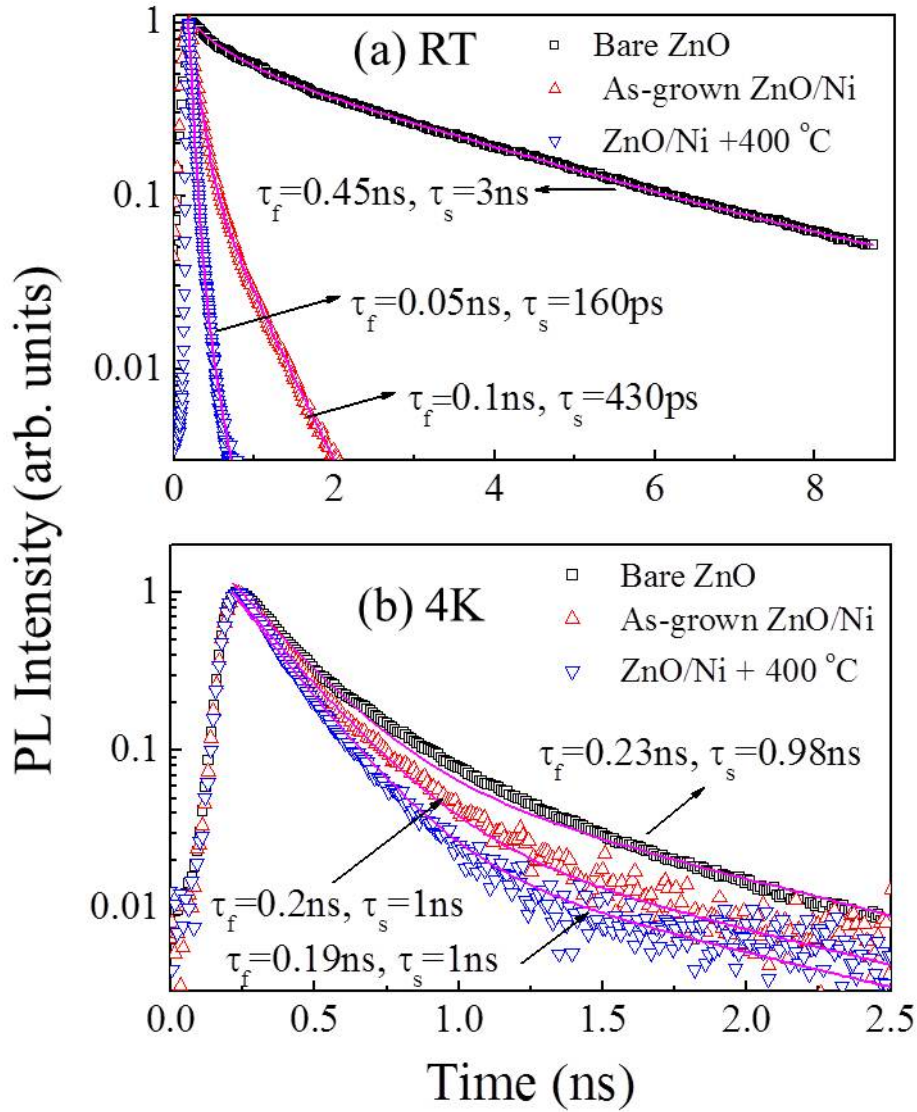


Figure 6. TRPL decays measured at room temperature (a) and 4K (b) from the ZnO NWs before and after Ni coating. The solid lines represent the bi-exponential fit to each decay curve with the fitting parameters as specified in the figure. In (b) the PL detecting energy was chosen at 3.3602 eV, i.e. at the peak position of the dominant BX emission. All PL decays are normalized to the same PL intensity.

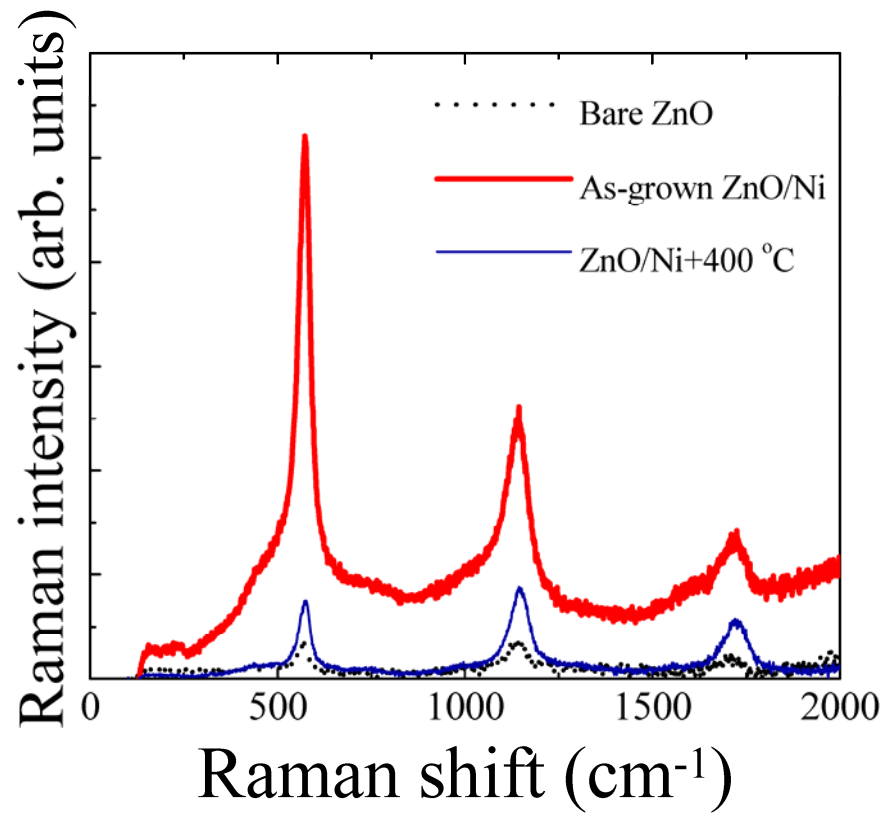


Figure 7. Representative Raman spectra measured from the ZnO NWs and ZnO/Ni core-shell structures.